Dissecting the Role of Substrate on the Morphology and Separation Properties of Thin Film Composite Polyamide Membranes: Seeing is Believing

Lu Elfa Peng,[†] Zhikan Yao,[‡] Zhe Yang,[†] Hao Guo,*[,†] Chuyang Y. Tang *[,†]

[†]Department of Civil Engineering, The University of Hong Kong, Pokfulam, Hong Kong SAR, China.

[‡]College of Chemical and Biological Engineering, Zhejiang University, Hangzhou, 310027, China.

*Corresponding Authors:

Hao Guo, guohao7@hku.hk, +852 28578470

Chuyang Y. Tang, tangc@hku.hk, +852 28591976

TABLE OF CONTENT

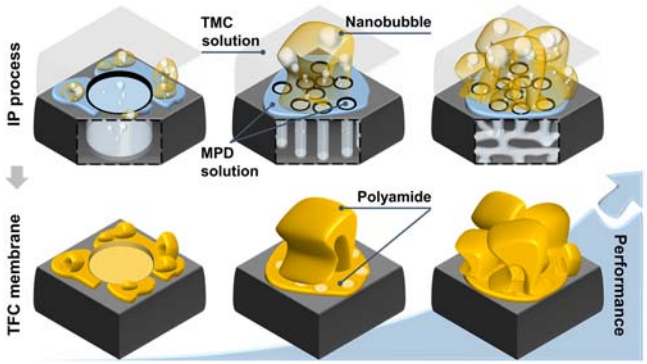

ABSTRACT

Recent studies show that the surface morphology of a thin film composite (TFC) polyamide membrane depends strongly on its porous substrate. Nevertheless, the underlining mechanisms and the effects on membrane separation performance remain controversial. To dissect the exact role of pore properties, we synthesized TFC polyamide membranes on polycarbonate substrates with cylindrical track-etched pores (PCTE) of well-defined pore size ranging from 10 to 800 nm. Leaf-like roughness features were most prominent for polyamide films formed on substrates of intermediate pore sizes (80 and 100 nm). Smaller pores inhibited leaf-like features as a result of insufficient storage of *m*-phenylenediamine (MPD) monomers for the interfacial reaction, whereas larger pores resulted in diminished surface roughness due to the lack of confinement to the interfacially degassed nanobubbles. Substrate porosity plays a critical role on membrane water permeability, while smaller pores with greater pore density are favored to improve membrane rejection. TFC polyamide membranes prepared on sponge-like polyethersulfone and polysulfone substrates exhibit better water permeability and salt rejection compared to the PCTE-TFC membranes, thanks to the simultaneously enhanced confinement and MPD storage effects. The mechanistic insights gained in this study reveals the huge potential of substrate design towards high performance TFC RO membranes.

INTRODUCTION

Researchers have been constantly questing for reverse osmosis (RO) membranes of better permeability and higher selectivity[1-4] to make them more competitive for desalination and water reuse.[5-8] Commercial RO membranes are generally prepared by an interfacial polymerization (IP) reaction between *m*-phenylenediamine (MPD) dissolved in water and trimesoyl chloride (TMC) dissolved in an organic solvent. Typically, a porous substrate saturated with MPD is brought into contact with the organic solution of TMC, which forms a thin cross-linked polyamide rejection film. Traditional wisdom often discounts the importance of substrate based on the simple belief that membrane separation performance is governed by the polyamide layer.[9-11] Nevertheless, recent studies revealed its critical influence on the morphology of the polyamide film[12-14] as well as its role in governing the hydraulic transport path within the composite membrane.[15-17] Improved membrane substrates have the potential to achieve an order of magnitude improvement in water permeability while maintaining the salt rejection.[18, 19]

Increasing number of studies have reported the influence of substrate properties (e.g. pore size,[12, 15, 20] pore densiy,[14] porosity,[13, 21, 22] and hydrophilicity[12, 21]) on the polyamide morphology. Nevertheless, their exact roles remain controversial. Several studies observed increased membrane surface roughness using substrates with larger pores,[12, 23, 24] yet others reported an opposite trend.[13, 18, 22] The effect of substrate on membrane separation performance is equally confusing. Singh et al.[15] reported that increasing the substrate pore size from 70 nm to 150 nm led to a thicker polyamide film with reduced water permeability. In contrast, Ghosh et al.[12] obtained more permeable membranes for relatively hydrophobic

substrates with larger pore diameters. These authors proposed a "volcano eruption" model to rationalize their results, i.e., a larger pore favors the eruption of its stored MPD, whose reaction with TMC forms a rough polyamide film spanning over the pore. Increased number of studies have also investigated the effect of surface porosity and pore density of the substrate.[13, 14, 16, 21, 22, 25] Furthermore, existing studies generally adopt substrates with a sponge-like skin, whose irregular surface pore structure complicates the decoupling of the individual effects of various substrate properties. These apparent deficits prompt us to perform a more systematic investigation to unveil the fundamental mechanisms governing the role of substrates.

Recent studies on advanced membrane characterization and formation mechanism of polyamide may provide us some useful hints. The polyamide film, with an apparent thickness on the order of 100 nm,[26-28] contains numerous nanovoids[29-31] such that its intrinsic thickness is as thin as 10-30 nm.[25, 32-34] Ma el al.[35, 36] revealed that these nanovoids are caused by interfacial degassing due to the release of H^+ and heat during the IP reaction. That is, the localized acidification and heating at the IP reaction interface converts the bicarbonate in the MPD solution (see Supporting Information S4) into CO_2 nanobubbles ($HCO_3^- + H^+ \xrightarrow{\Delta} CO_2\uparrow + H_2O$). These nanobubbles are encapsulated within the polyamide film, which forms its "leaves and nodules" morphology.[25, 35-37] Song et al.[38] further demonstrates the importance of confinement conditions: the roughness features of leaves and nodules disappeared for polyamide films prepared at a free interface. The lack of substrate in this case allows the degassed nanobubbles to freely escape from the interface, in contrast to the conventional case that nanobubbles are confined between the substrate

and the polyamide film. Presumably, the confinement effect will be significantly weakened with larger substrate pore size (e.g., a free interface can be idealized as a substrate with infinitely large pore size), which can provide a new and unique angle to interpret the role of substrates.

To dissect the role of substrates on the formation of polyamide morphology, we selected polycarbonate membranes with track-etched cylindrical pores (PCTE). Additional substrates were also included for comparison purpose, including polyethersulfone (PES) and polysulfone (PSf) substrates prepared by phase inversion, and nanofibrous polyacrylonitrile (PAN) substrate prepared by electrospinning. We carefully characterized the membrane morphology and separation properties, which provides deep insights on the critical role of substrate during IP reaction.

MATERIALS AND METHODS

Chemicals and membrane substrates. Chemicals used for membrane preparation, including MPD (99%), TMC (98%), n-hexane (HPLC grade), PSf (Mw ~ 35000), and dimethylformamide (DMF, anhydrous 99.8%) were all obtained from Sigma-Aldrich. Other chemicals, including tetrahydrofuran and sodium chloride (NaCl) were purchased from Dieckmann. PCTE were supplied by Sterlitech. These substrates have uniform cylindrical pores, with nominal pore size ranging from 10 to 800 nm. They are denoted as PCTE-10 to PCTE-800 in accordance to their nominal pore size. Other commercial substrates used in this study include a nanofibrous PAN prepared by electronspinning (Sterlitech) and two PES substrates prepared by phase inversion (PES1 from Synder and PES2 from Sterlitech). An additional PSf substrate was prepared in-house by phase inversion as described in our previous works.[37, 39] Detailed properties of these substrates are summarized in Table 1.

Fabrication of TFC polyamide RO membranes. TFC membranes were prepared by performing IP reaction on various substrates. Briefly, a substrate was first soaked in 1 wt. % aqueous MPD solution for 2 min. After removing excess MPD solution by a rubber roller, a 0.1 wt. % TMC/hexane solution was applied to the MPD-impregnated substrate for 1 min to form polyamide. The resultant polyamide membrane was rinsed by hexane and kept in 50 ℃ water bath for 10-min for further polymerization. The TFC membranes formed on PCTE substrates are denoted as TFC-10 to TFC-800 based on the nominal pore size of the substrates, and those made on commercial/homemade substrates are named as TFC-PES1, TFC-PES2, TFC-PSf, and TFC-PAN according to the type of substrate used.

Membrane characterization. Field-emission scanning electron microscopy (FE-SEM, S-4800, Hitachi) was used to characterize membrane morphology. All SEM samples were dried and sputter-coated with a thin layer of gold. To obtain the bottom surface of the polyamide layer, the substrate was removed by gently dripping a suitable solvent, i.e., tetrahydrofuran for dissolving PCTE or DMF for dissolving PES, PSf, and PAN. The isolated polyamide layer was placed on a silicon wafer with bottom surface-side up and thoroughly dried before further characterization.

Membrane separation performance. Membrane performance including water flux and salt (NaCl) rejection were tested using a laboratory-scale cross-flow RO filtration system as detailed in the previous work.[37] The effective filtration area of each membrane coupon was 12.0 cm^2. After pre-compaction at 17.0 bar for 2 h, the membrane coupon was tested using a 2000 ppm NaCl feed solution at 15.5 bar with a cross-flow velocity of 22.4 cm/s under room temperature (~25 °C). The water flux J_v and permeability A are calculated by:

$$J_v = \frac{\Delta m}{\Delta t \times a \times \rho} \quad (1)$$

$$A = \frac{J_v}{\Delta P - \Delta \pi} \quad (2)$$

where Δm is the mass of permeate over a time interval of Δt, a is the effective membrane area, ρ is the density of water, ΔP is the transmembrane pressure, and $\Delta \pi$ is the transmembrane osmotic pressure.

NaCl concentrations in the feed and the permeate (i.e., C_f and C_p, respectively) were determined based on conductivity measurements (Ultrameter II, Myron L). NaCl rejection (R) was calculated by:

$$R = \frac{C_f - C_p}{C_f} \times 100\% \quad (3)$$

RESULTS AND DISCUSSION

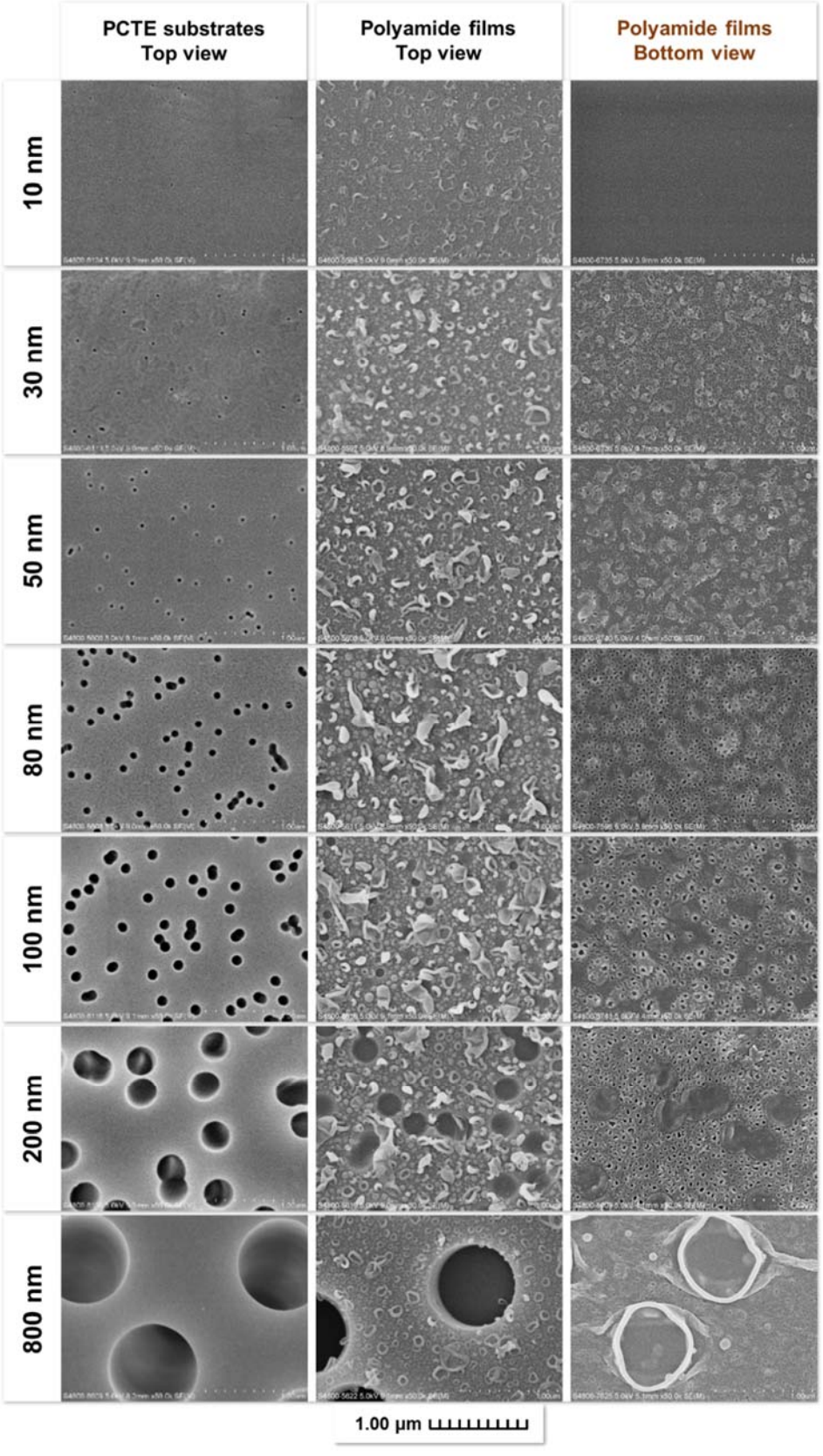

Figure 1. SEM micrographs of the PCTE substrates and the top and bottom views of polyamide films for the corresponding TFC membranes. Scale bar = 1.00 μm.

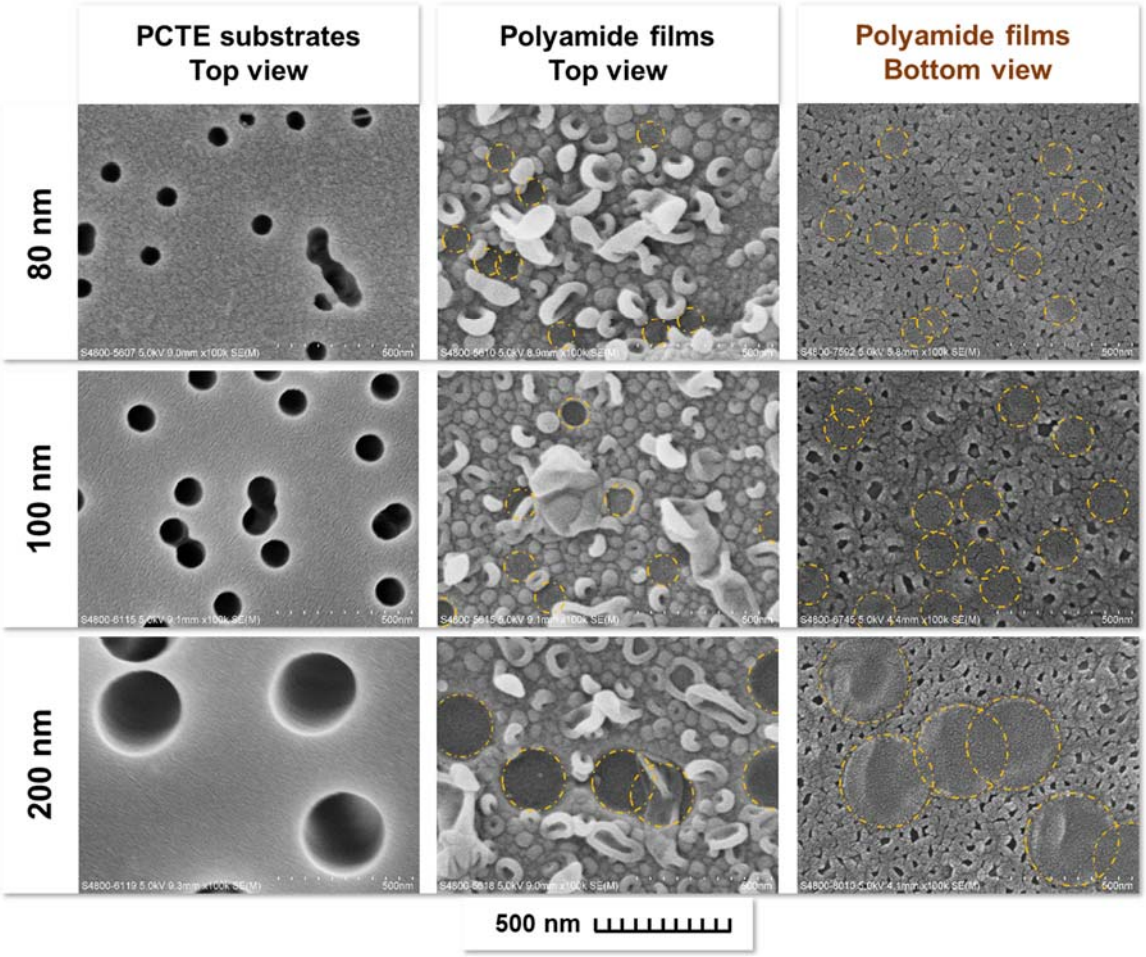

Figure 2. Magnified SEM micrographs of PCTE substrates surface (PCTE-80, PCTE-100, and PCTE-200) and the top and bottom views of polyamide films for the corresponding TFC membranes (TFC-80, TFC-100, and TFC-200). Scale bar = 500 nm.

Table 1. Properties of substrates used in the current study.

	PCTE							PES1	PSf	PES2	PAN
Nominal size [a]	10 nm	30 nm	50 nm	80 nm	100 nm	200 nm	800 nm	300 kDa	NA	30 nm	200 nm
Observed size (in diameter) (nm) [b]	13 ± 4	28 ± 2	40 ± 5	72 ± 6	106 ± 4	270 ± 12	890 ± 20	16 ± 4	35 ± 12	186 ± 122	NA
Pore density (counts/μm^2) [b]	8 ± 1	5 ± 1	10 ± 2	14 ± 1	11 ± 1	4 ± 1	1 ± 1	307 ± 55	325 ± 16	8 ± 2	NA
Surface porosity (%) [b]	0.1	0.4	2.0	7.2	8.6	8.6	25.1	6.2	31.3	21.2	NA

Note:

a. Provided by manufacturer.

b. Based on SEM characterization (see more details in Supporting Information S1).

TFC membranes formed on PCTE. Figure 1 presents the SEM micrographs of the PCTE substrates (top view) and the polyamide films (both top and bottom views). It is important to note that the actual pore size of PCTE-200 and PCTE-800 was approximately 70 - 90 nm larger than the respective nominal sizes provided by the manufacturer (Table 1). The nominal size of other PCTE substrates were reasonably accurate. The top surfaces of polyamide films show leaf-like roughness features, whose presence were most obvious for TFC-80 and TFC-100. Increasing the substrate pore size from 100 nm to 800 nm led to the diminishing of these characteristic features. According to our recent works,[35] the leaf-like features were formed due to the interfacial degassing of CO_2 nanobubbles that are encapsulated between the polyamide film and the substrate. Increasing the pore size of the substrate would reduce the confinement effect by the substrate and allow the nanobubbles to escape through the large pores.[38] In contrast to the common belief that leaves grow directly over pores,[12, 20] we observed smooth and flat polyamide films spanning over the pores of 80-200 nm (highlighted by dotted circles in Figure 2). Indeed, the leaf-like features developed predominantly around the pores. Although these observations appear to be

peculiar and counter-intuitive, they are consistent with the interfacial degassing theory.[35, 37, 38] Due to the release of heat and H^+ during the IP reaction, the dissolved bicarbonate will be degassed (see ref.[37] and Supporting Information S4). This degassing can possibly happen both inside the substrate pores and at the vicinity of the pores. The confinement effect by the solid matrix around the pores allows the CO_2 nanobubbles to be retained, which shapes the leaf-like roughness features.[38] However, the confinement effect was the weakest directly over the straight cylindrical pores, which prevents the effective retention of degassed nanobubbles. Therefore, our study further confirms the critical importance of the substrate confinement effect in shaping the polyamide surface roughness. This confinement effect also explains why surface roughness could not effectively develop for polyamide films formed at free interfaces.[32, 38, 40] With a further increase of substrate pore size to 800 nm, the polyamide intruded into the substrate due to a lack of effective support (see the bottom view of TFC-800 in Figure 1).

Interestingly, increasing the substrate pore size from 10 to 80 nm led to an opposite trend. While the roughness features were barely noticeable for TFC-10, they became increasingly larger for TFC-30, TFC-50 and TFC-80. This trend can possibly be rationalized by the greater storage of MPD (Supporting Information S4) and its enhanced diffusion with the increasing pore size.[13, 15] According to the interfacial degassing theory, increasing the effective concentration of MPD would cause greater production of heat at the reaction interface to promote the release of CO_2 nanobubbles.[35] Our observation is also consistent with some earlier studies reporting increased roughness formation for larger pores.[12, 23, 24, 40] Some of the earlier studies attributed the greater roughness to the enhanced “volcanic”

eruption of MPD.[12, 41, 42] However, this eruption model alone (which would predict the greatest roughness for TFC-800 as well as the formation of roughness features directly over pores) cannot fully explain the surface morphology of the polyamide film. In the current study, we demonstrate that this surface morphology is governed by two competing mechanisms, with larger pores leading to reduced confinement effect (a roughness inhibitor) in addition to greater MPD storage (a roughness promoter).

Consistent with previous reports,[22, 25, 38, 43] we observed "honeycomb-like" pore openings over the bottom side of the polyamide films (Figure 1 and Figure 2). The size and number density of these openings (Table S1) appear to be well correlated to the surface roughness. For example, TFC-80 had the greatest number density (323 ± 30 counts/μm^2), which was approximately an order of magnitude higher than that of TFC-30 and TFC-800. For the case of TFC-10, such back-side openings cannot be clearly identified. According to Song et al.,[25, 38] the growth of nanobubbles shapes the surface roughness of the film, while their forced escape from the backside of the polyamide leaves the "honeycomb-like" openings behind. It is interesting to note the absence of such openings for polyamide formed directly over the large substrate pores where the confinement effect was the weakest (TFC-80, TFC-100 and TFC-200, Figure 2).

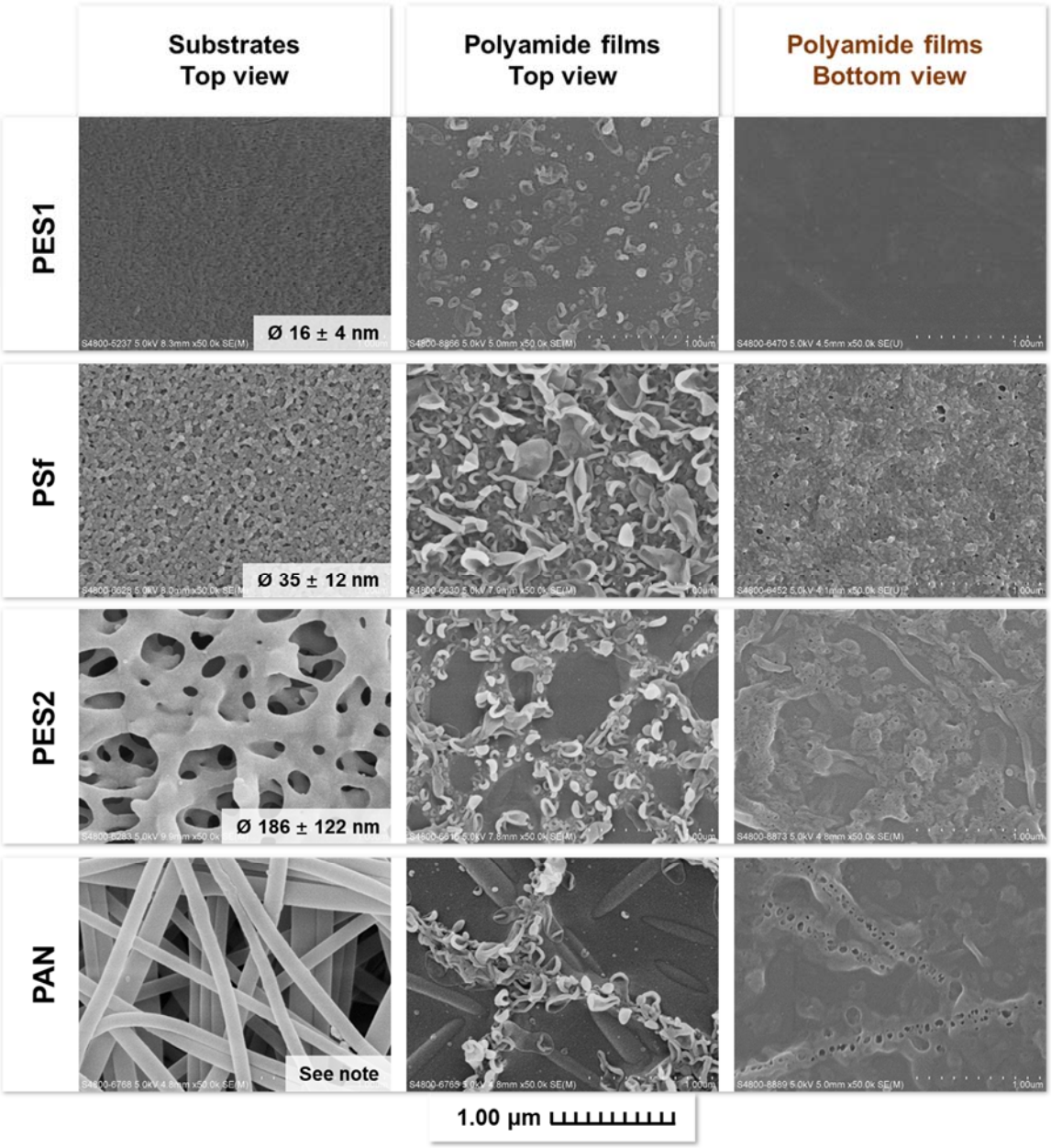

222

223 **Figure 3.** SEM micrographs of commercial/homemade substrates and the top and bottom views of
224 polyamide films of the corresponding TFC membranes (TFC-PES1, TFC-PSf, TFC-PES2 and TFC-
225 PAN). Scale bar = 1.00 µm. Note: the electrospun PAN substrate had less well-defined pores with
226 irregular shape.

227

228 **TFC membranes formed on other substrates.** Figure 3 presents SEM micrographs of

229 TFC membranes prepared on other types of substrates, i.e., PES1, PSf, PES2 and PAN in

230 increasing surface pore size. Consistent with the results for PCTE substrates, roughness

features could not effectively develop directly over large pores (>>100 nm) of the electrospun nanofibrous PAN. Similarly, leaf-like features could not be found over the large pores of PES2 (prepared by conventional phase inversion). These observations further underpin the role of confinement on roughness formation. Indeed, the leaf-like features of TFC-PES2 and TFC-PAN concentrated over the solid polymeric regions of their substrates where the confinement effect would be the strongest. The PSf substrate, with an average pore size of 35 ± 12 nm, had the most prominent "leaves and nodules" appearance. In contrast, PES1 with smaller pore size presents smaller roughness features, possibly due to the reduced storage of MPD. In addition to the substrate pore structure, other factors such as the surface hydrophilicity, morphology and specific chemistry of the substrate may not neglected.[12, 44, 45] For example, increased substrate hydrophobicity appears to reduce the formation of leaf-like roughness features (Supporting Information S3), which is likely due to reduced capillary effect and thus reduced MPD uptake by the substrate. Furthermore, the use of some specific chemistry may also significantly increase the MPD uptake (e.g., due to hydrogen bonding).[19, 46] Future studies on the influence of the surface roughness of the substrate on polyamide morphology is also needed.

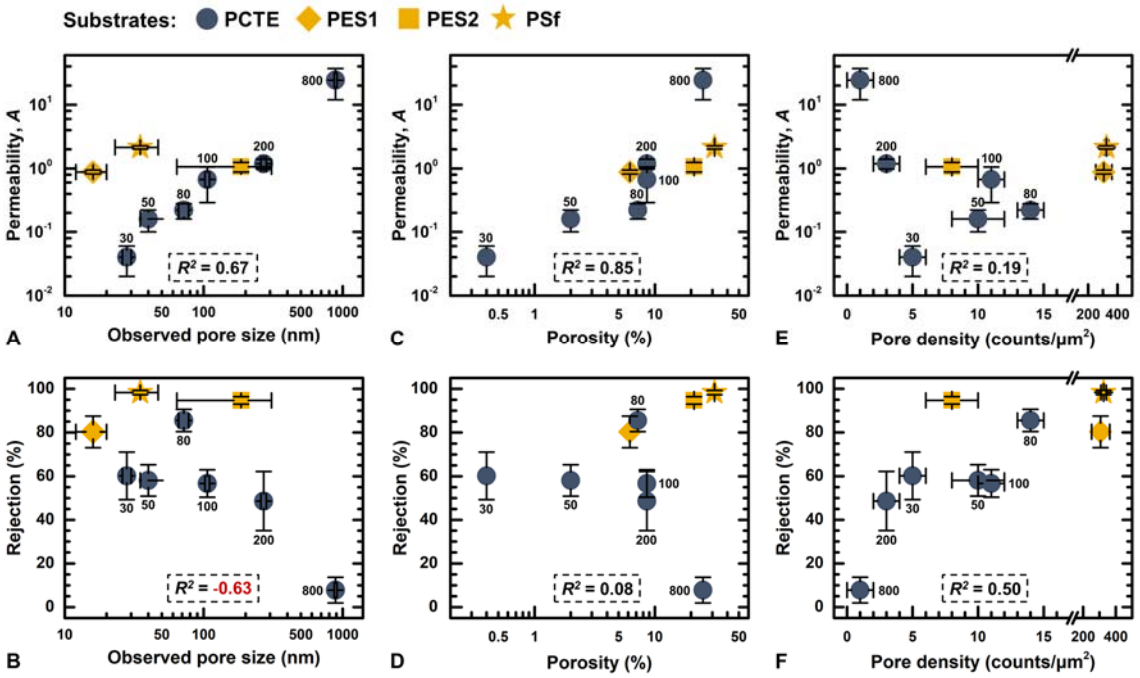

Figure 4. Correlations between pore properties of substrates with the separation performance of the TFC membranes. Note: TFC-10 did not show any water permeability. On the other hand, TFC-PAN had nearly zero rejection against NaCl, implying the failure to form an intact rejection layer. Therefore, these two membranes were excluded from the correlation analysis. PCTE substrates are labeled using the corresponding nominal pore size, while the measured pore size (Table 1) is used in the figure. R^2 is the correlation coefficient obtained from Microsoft Excel between separation properties (rejection or log(permeability in $Lm^{-2}h^{-1}bar^{-1}$)) and pore properties (log(pore size), log(porosity), or pore density).

Effect of substrate pore properties on membranes separation performance. Figure 4 presents the effect of substrate pore size, porosity and pore density on the permeability and rejection of the TFC membranes. For the PCTE substrates, increasing substrate pore size had an obvious positive effect in increasing the TFC membrane permeability (Figure 4A). However, the membrane rejection can be seriously comprised for cylindrical pores of greater than 100 nm in size (Figure 4B), possibly due to the greater tendency to form more defects in the polyamide layer over large substrate pores.[19] In addition, for the ultrathin and supported polyamide film that spans over the large cylindrical pores of PCTE substrates, it is mechanically unstable (e.g., the thin film is stretched due to the tensile stress in longitudinal direction when the membrane is pressurized, causing a loss of membrane

integrity [47, 48]). Compared to the PCTE counterparts, the corresponding PES and PSf substrates with comparable pore sizes showed better combinations of permeability and rejection, implying that substrates with sponge-like structures are preferred for interfacial polymerization. Notably, the much improved permeabilities of TFC-PES1 and TFC-PSf (average substrate pore sizes of 16 ± 4 nm and 35 ± 12 nm, respectively) over their TFC-PCTE counterparts of similar pore size range (10-50 nm) can be explained by the substantially higher surface porosity for sponge-like substrates. Indeed, Figure 4C shows a much better correlation between permeability and porosity (R^2 = 0.85), revealing substrate surface porosity as a more important parameter than pore size in governing the permeability of the resulting TFC membrane. Our work is in good agreement with the existing literature that high-porosity substrates are favored to reduce the hydraulic resistance for water transport through the polyamide layer.[14-17] In the current study, the correlation between the TFC permeability and substrate pore density (R^2 = 0.19) was much weaker (Figure 4E).

Despite the overall good correlation between membrane permeability and substrate porosity, it is important to note its inherent limitations. For example, TFC-800 had a very low NaCl rejection of < 10%, which was likely caused by either defects formed during membrane formation or mechanical damages due to the applied pressure during membrane testing. These defects or mechanical damages may lead to artificially increased permeability (Supporting Information S5), which possibly explains why TFC-800 deviates significantly from the overall trend established by the other datapoints in Figure 4C. Furthermore, the much improved permeabilities of TFC-PES1 and TFC-PSf over their TFC-PCTE counterparts of similar pore size range may not be completely explained by the

substantially higher surface porosity for sponge-like substrates, since membrane permeability can also be potentially affected by the type of materials and pore morphology. Future studies are needed to further investigate these factors.

Unlike membrane permeability that shows the greatest dependence on substrate porosity (R^2 = 0.85, Figure 4C), the dependence of rejection on substrate porosity was more disparate (R^2 = 0.08, Figure 4D). While some high-porosity TFC-PCTE membranes suffered from low rejections, increasing porosity appears to enhance rejection for membranes prepared on sponge-like PES and PSf substrates. In general, membranes formed on PES and PSf had much higher rejection than TFC-PCTE membranes. For the PCTE substrates, higher porosity was mainly due to the increased pore size (Table 1). For the PES and PSf substrates, increasing porosity can be achieved by the combination of greater pore size and higher pore density. In the current study, larger pore size tends to cause lower rejection (Figure 4B) while greater pore density favors better rejection (Figure 4F).

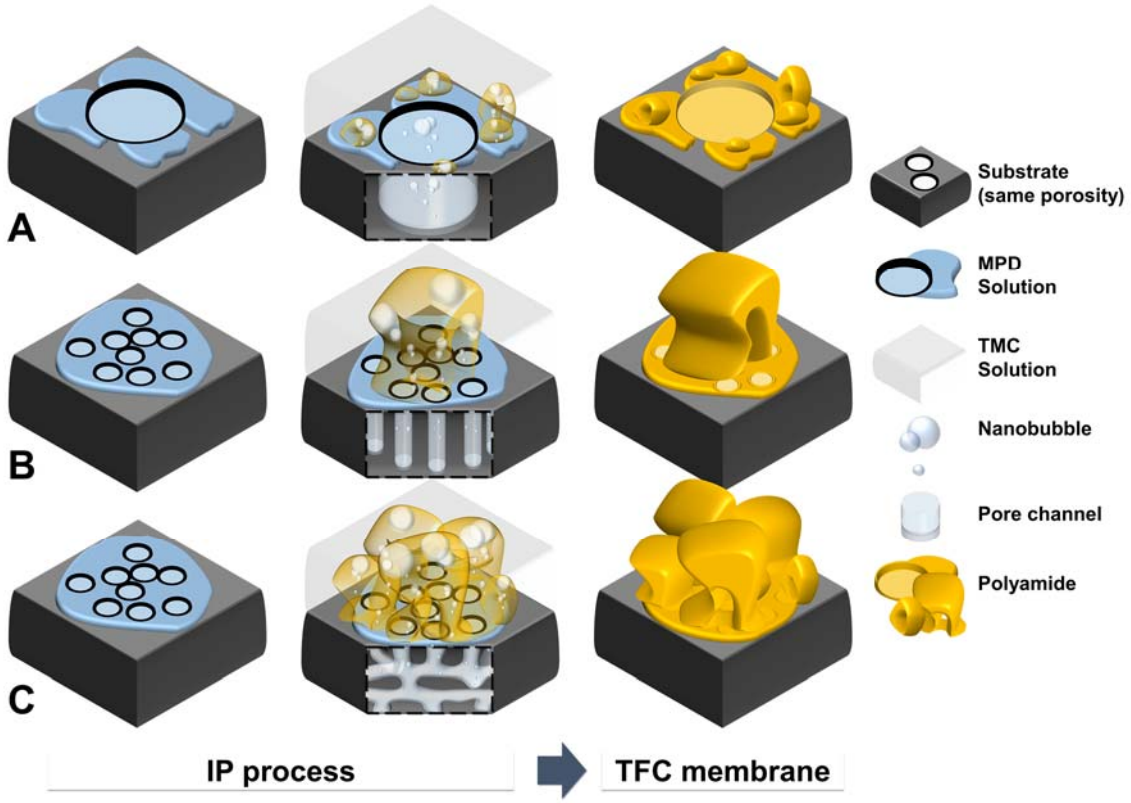

306
307

308 **Figure 5.** Conceptional illustration of the role of substrate on interfacial polymerization.

309

310 **Mechanistic insights and future perspectives.** The current study highlights two
311 important roles of the substrates during the formation of polyamide rejection films: the
312 storage of MPD monomers and the provision of confinement to interfacially degassed
313 nanobubbles. Although increasing pore size is favorable to increase the MPD storage
314 (Supporting Information S4), it results in a simultaneous loss of the confinement effect
315 (Figure 5A). For example, even though the amount of dissolved CO_2 in the PCTE-800
316 substrate was nearly double of that in the PSf substrate (Supporting Information S4),
317 PCTE-800 was less effective to form roughness features over its large sized pores (Figure
318 1). For such substrates containing pores, nodules and leaf-like features appeared
319 predominately over the solid polymeric areas adjacent to the pore region. According to our

prior studies, confined nanobubbles tend to deliver MPD monomers to the reaction front due to the convention under a pressure gradient, which favors the sealing of defects in polyamide films formed under mild interfacial degassing.[25] In contrast, the lack of confinement results in polyamide films with more defects and lower salt rejection.[38] In addition to the loss of confinement, large substrate pores may further lead to undesirable intrusion of polyamide into the substrate pores (Figure 2 and Ref.[19]). Thin films spanning over larger unsupported distance are also less mechanically stable, especially under high applied mechanical pressure.[47]

Our study further implies that substrates with greater number of smaller pores are favored over those with fewer numbers of larger pores in order to achieve better salt rejection without scarifying permeability. In this combination, the large pore density helps to maintain the desired surface porosity (thus MPD storage during the interfacial reaction and path for water permeation in the resultant membrane), and the smaller substrate pore size ensures proper confinement effect and high membrane rejection (Figure 5B). Coincidentally, a modelling work by Ramon et al.[16] also suggested that greater number of smaller pores are more favorable to minimize the average transport distance through the polyamide film, noting that their work implicitly assumes that the formation of polyamide film itself is not affected by the substrate pore structures. Our work demonstrates that, although nodules and leaf-like features cannot be effectively developed over large pores of ~ or > 100 nm, these roughness features can be formed over smaller pores as a result of stronger confinement effect. For densely packed small pores, it is likely that a cluster of neighboring substrate pores act together for the formation of roughness features. That is,

MPD is released from these pores, whose reaction with TMC forms degassed nanobubbles that are effectively retained by the substrate (due to the greater resistance to air passage with the presence of solid regions and smaller pore size) to shape the formation of roughness features. This hypothesis is supported by several recent studies: (1) microscopic characterization of commercial TFC membranes reveals that each roughness nodule spans over multiple substrate pores,[20, 25, 38] and (2) tracer filtration tests confirm that the nanovoids contained in roughness nodules are directly connected to the substrate pores.[25, 49]

Although this study used PCTE substrates to dissect the role of substrate pores, the TFC membranes prepared on conventional PES and PSf substrates showed much better combinations of permeability and rejection, underpinning the preference of substrates with higher porosity, greater pore density yet smaller pore size. In addition, PES and PSf substrates could further enhance the MPD storage (due to their sponge-like and asymmetric structure to serve as a better reservoir for MPD) and the confinement effect (due to the tortuous pores and therefore greater resistance to degassed nanobubbles) (Figure 5C). Following these criteria, coating a microporous interlayer on a conventional substrate may be highly beneficial to further enhance MPD uptake[19] as well as the gas confinement effect. Indeed, several studies have demonstrated one order of magnitude improvement in membrane permeability by the simple incorporation of an interlayer.[19, 50] The current study, in concert with other recent literature studies, reveals the huge potential for further optimization of TFC RO membranes as well as the critical need to conduct more systematic and mechanistic studies on the fundamental roles of membrane substrates.

The current study along with other recent membrane characterization works[25, 29-34] also provide important inputs to the development of more accurate simulation studies on the formation of polyamide RO membranes. For example, recent studies on multiscale molecular simulation predict an intrinsic film thickness on the order of 10 nm for polyamide formed by the IP reaction of MPD and TMC,[51, 52] which agrees reasonably well with electron microscopic characterization results.[25, 32-34] Nevertheless, the simulated surface roughness of 1 – 4 nm [52] was two orders of magnitude below the typical values for fully aromatic polyamide membranes.[25, 33, 34, 53] Future simulation studies should consider the inclusion of the interfacial degassing mechanism[25, 35-38] in order to provide more accurate predictions of surface roughness.

SUPPORTING INFORMATION

S1. Determination of pore density and porosity; S2 Properties of the backside openings of polyamide films; S3 Effect of hydrophilicity of substrates; S4 Theoretical calculations for CO_2 degassing; S5. Resolving the intrinsic permeability of TFC-PCTE membrane. This material is available free of charge via the Internet at http://pubs.acs.org.

ACKNOWLEDGMENTS

The work is partially supported by a grant from the Research Grants Council of the Hong Kong Special Administration Region, China (C7051-17G).

REFERENCES

1. Lee, K. P.; Arnot, T. C.; Mattia, D., A review of reverse osmosis membrane materials for desalination—Development to date and future potential. *J. Membr. Sci.* **2011,** *370*, (1-2), 1-22.

2. Park, H. B.; Kamcev, J.; Robeson, L. M.; Elimelech, M.; Freeman, B. D., Maximizing the right stuff: The trade-off between membrane permeability and selectivity. *Science* **2017,** *356*, (6343), eaab0530.

3. Qasim, M.; Badrelzaman, M.; Darwish, N. N.; Darwish, N. A.; Hilal, N., Reverse osmosis desalination: A state-of-the-art review. *Desalination* **2019,** *459*, 59-104.

4. Yang, Z.; Guo, H.; Tang, C. Y. Y., The upper bound of thin-film composite (TFC) polyamide membranes for desalination. *J. Membr. Sci.* **2019,** *590*, 117297.

5. Greenlee, L. F.; Lawler, D. F.; Freeman, B. D.; Marrot, B.; Moulin, P., Reverse osmosis desalination: water sources, technology, and today's challenges. *Water Res.* **2009,** *43*, (9), 2317-48.

6. Xie, M.; Shon, H. K.; Gray, S. R.; Elimelech, M., Membrane-based processes for wastewater nutrient recovery: Technology, challenges, and future direction. *Water Res.* **2016,** *89*, 210-21.

7. Tang, C. Y.; Yang, Z.; Guo, H.; Wen, J. J.; Nghiem, L. D.; Cornelissen, E., Potable Water Reuse through Advanced Membrane Technology. *Environ. Sci. Technol.* **2018,** *52*, (18), 10215-10223.

8. Lin, S., Energy Efficiency of Desalination: Fundamental Insights from Intuitive Interpretation. *Environ. Sci. Technol.* **2020,** *54*, (1), 76-84.

9. Hirose, M.; Ito, H.; Kamiyama, Y., Effect of skin layer surface structures on the flux behaviour of RO membranes. *J. Membr. Sci.* **1996,** *121*, (2), 209-215.

10. Mulder, M., *Basic principles of membrane technology*. 2nd ed.; Kluwer Academic: Dordrecht; Boston, 1996; p 564 p.

11. Kim, S. H.; Kwak, S. Y.; Suzuki, T., Positron annihilation spectroscopic evidence to demonstrate the flux-enhancement mechanism in morphology-controlled thin-film-composite (TFC) membrane. *Environ. Sci. Technol.* **2005,** *39*, (6), 1764-1770.

12. Ghosh, A. K.; Hoek, E. M. V., Impacts of support membrane structure and chemistry on polyamide–polysulfone interfacial composite membranes. *J. Membr. Sci.* **2009,** *336*, (1-2), 140-148.

13. Huang, L.; McCutcheon, J. R., Impact of support layer pore size on performance of thin film composite membranes for forward osmosis. *J. Membr. Sci.* **2015,** *483*, 25-33.

14. Li, X. S.; Li, Q.; Fang, W. X.; Wang, R.; Krantz, W. B., Effects of the support on the characteristics and permselectivity of thin film composite membranes. *J. Membr. Sci.* **2019,** *580*, 12-23.

15. Singh, P. S.; Joshi, S. V.; Trivedi, J. J.; Devmurari, C. V.; Rao, A. P.; Ghosh, P. K., Probing the structural variations of thin film composite RO membranes obtained by coating polyamide over polysulfone membranes of different pore dimensions. *J. Membr. Sci.* **2006,** *278*, (1-2), 19-25.

16. Ramon, G. Z.; Wong, M. C. Y.; Hoek, E. M. V., Transport through composite membrane, part 1: Is there an optimal support membrane? *J. Membr. Sci.* **2012,** *415-416*, 298-305.

17. Wijmans, J. G.; Hao, P., Influence of the porous support on diffusion in composite membranes. *J. Membr. Sci.* **2015,** *494*, 78-85.

18. Park, S.-J.; Choi, W.; Nam, S.-E.; Hong, S.; Lee, J. S.; Lee, J.-H., Fabrication of polyamide thin film composite reverse osmosis membranes via support-free interfacial polymerization. *J. Membr. Sci.* **2017,** *526*, 52-59.

19. Yang, Z.; Zhou, Z. W.; Guo, H.; Yao, Z.; Ma, X. H.; Song, X.; Feng, S. P.; Tang, C. Y., Tannic Acid/Fe(3+) Nanoscaffold for Interfacial Polymerization: Toward Enhanced Nanofiltration Performance. *Environ. Sci. Technol.* **2018,** *52*, (16), 9341-9349.

20. Yan, H.; Miao, X.; Xu, J.; Pan, G.; Zhang, Y.; Shi, Y.; Guo, M.; Liu, Y., The porous structure of the fully-aromatic polyamide film in reverse osmosis membranes. *J. Membr. Sci.* **2015,** *475*, 504-510.

21. Ding, C.; Yin, J.; Deng, B., Effects of polysulfone (PSf) support layer on the performance of thin-film composite (TFC) membranes. *J. Chem. Proc. Eng.* **2014,** *1*, 1-8.

22. Wang, J.; Xu, R.; Yang, F.; Kang, J.; Cao, Y.; Xiang, M., Probing influences of support layer on the morphology of polyamide selective layer of thin film composite membrane. *J. Membr. Sci.* **2018,** *556*, 374-383.

23. Song, Y.; Sun, P.; Henry, L.; Sun, B., Mechanisms of structure and performance controlled thin film composite membrane formation via interfacial polymerization process. *J. Membr. Sci.* **2005,** *251*, (1-2), 67-79.

24. Ehsan Yakavalangi, M.; Rimaz, S.; Vatanpour, V., Effect of surface properties of polysulfone support on the performance of thin film composite polyamide reverse osmosis membranes. *J. Appl. Polym. Sci.* **2016,** *134*, (6), 44444.

25. Song, X.; Gan, B.; Qi, S.; Guo, H.; Tang, C. Y.; Zhou, Y.; Gao, C., Intrinsic Nanoscale Structure of Thin Film Composite Polyamide Membranes: Connectivity, Defects, and Structure-Property Correlation. *Environ. Sci. Technol.* **2020,** *54*, (6), 3559-3569.

26. Elimelech, M.; Zhu, X. H.; Childress, A. E.; Hong, S. K., Role of membrane surface morphology in colloidal fouling of cellulose acetate and composite aromatic polyamide reverse osmosis membranes. *J. Membr. Sci.* **1997,** *127*, (1), 101-109.

27. Tang, C. Y. Y.; Kwon, Y. N.; Leckie, J. O., Probing the nano- and micro-scales of reverse osmosis membranes - A comprehensive characterization of physiochemical properties of uncoated and coated membranes by XPS, TEM, ATR-FTIR, and streaming potential measurements. *J. Membr. Sci.* **2007,** *287*, (1), 146-156.

28. Kong, C.; Kanezashi, M.; Yamomoto, T.; Shintani, T.; Tsuru, T., Controlled synthesis of high performance polyamide membrane with thin dense layer for water desalination. *J. Membr. Sci.* **2010,** *362*, (1-2), 76-80.

29. Pacheco, F. A.; Pinnau, I.; Reinhard, M.; Leckie, J. O., Characterization of isolated polyamide thin films of RO and NF membranes using novel TEM techniques. *J. Membr. Sci.* **2010,** *358*, (1-2), 51-59.

30. Pacheco, F.; Sougrat, R.; Reinhard, M.; Leckie, J. O.; Pinnau, I., 3D visualization of the internal nanostructure of polyamide thin films in RO membranes. *J. Membr. Sci.* **2016,** *501*, 33-44.

31. Lin, L.; Lopez, R.; Ramon, G. Z.; Coronell, O., Investigating the void structure of the polyamide active layers of thin-film composite membranes. *J. Membr. Sci.* **2016,** *497*, 365-376.

32. Karan, S.; Jiang, Z. W.; Livingston, A. G., Sub-10 nm polyamide nanofilms with ultrafast solvent transport for molecular separation. *Science* **2015,** *348*, (6241), 1347-1351.

33. Kłosowski, M. M.; McGilvery, C. M.; Li, Y.; Abellan, P.; Ramasse, Q.; Cabral, J. T.; Livingston, A. G.; Porter, A. E., Micro-to nano-scale characterisation of polyamide structures of the SW30HR RO membrane using advanced electron microscopy and stain tracers. *J. Membr. Sci.* **2016,** *520*, 465-476.

34. Song, X.; Smith, J. W.; Kim, J.; Zaluzec, N. J.; Chen, W.; An, H.; Dennison, J. M.; Cahill, D. G.; Kulzick, M. A.; Chen, Q., Unraveling the Morphology-Function Relationships of Polyamide Membranes Using Quantitative Electron Tomography. *ACS Appl Mater Interfaces* **2019,** *11*, (8), 8517-8526.

35. Ma, X.-H.; Yao, Z.-K.; Yang, Z.; Guo, H.; Xu, Z.-L.; Tang, C. Y.; Elimelech, M., Nanofoaming of Polyamide Desalination Membranes To Tune Permeability and Selectivity. *Environ. Sci. Technol. Lett.* **2018,** *5*, (2), 123-130.

36. Ma, X.; Yang, Z.; Yao, Z.; Guo, H.; Xu, Z.; Tang, C. Y., Tuning roughness features of thin film composite polyamide membranes for simultaneously enhanced permeability, selectivity and anti-fouling performance. *J. Colloid Interface Sci.* **2019,** *540*, 382-388.

37. Peng, L. E.; Yao, Z.; Liu, X.; Deng, B.; Guo, H.; Tang, C. Y., Tailoring Polyamide Rejection Layer with Aqueous Carbonate Chemistry for Enhanced Membrane Separation: Mechanistic Insights, Chemistry-Structure-Property Relationship, and Environmental Implications. *Environ. Sci. Technol.* **2019,** *53*, (16), 9764-9770.

38. Song, X.; Gan, B.; Yang, Z.; Tang, C. Y.; Gao, C., Confined nanobubbles shape the surface roughness structures of thin film composite polyamide desalination membranes. *J. Membr. Sci.* **2019,** *582*, 342-349.

39. Yao, Z.; Guo, H.; Yang, Z.; Qing, W.; Tang, C. Y., Preparation of nanocavity-contained thin film composite nanofiltration membranes with enhanced permeability and divalent to monovalent ion selectivity. *Desalination* **2018,** *445*, 115-122.

40. Jiang, Z.; Karan, S.; Livingston, A. G., Water Transport through Ultrathin Polyamide Nanofilms Used for Reverse Osmosis. *Adv. Mater.* **2018,** *30*, (15), 1705973.

41. Li, X.; Wang, K. Y.; Helmer, B.; Chung, T.-S., Thin-Film Composite Membranes and Formation Mechanism of Thin-Film Layers on Hydrophilic Cellulose Acetate Propionate Substrates for Forward Osmosis Processes. *Ind. Eng. Chem. Res.* **2012,** *51*, (30), 10039-10050.

42. Liu, B.; Chen, C.; Zhao, P.; Li, T.; Liu, C.; Wang, Q.; Chen, Y.; Crittenden, J., Thin-film composite forward osmosis membranes with substrate layer composed of polysulfone blended with PEG or polysulfone grafted PEG methyl ether methacrylate. *Frontiers Chemi. Sci. Eng.* **2016,** *10*, (4), 562-574.

43. Xu, J.; Yan, H.; Zhang, Y.; Pan, G.; Liu, Y., The morphology of fully-aromatic polyamide separation layer and its relationship with separation performance of TFC membranes. *J. Membr. Sci.* **2017,** *541*, 174-188.

44. Jimenez-Solomon, M. F.; Gorgojo, P.; Munoz-Ibanez, M.; Livingston, A. G., Beneath the surface: Influence of supports on thin film composite membranes by interfacial polymerization for organic solvent nanofiltration. *J. Membr. Sci.* **2013,** *448*, 102-113.

45. Yao, Z.; Guo, H.; Yang, Z.; Lin, C.; Zhu, B.; Dong, Y.; Tang, C. Y., Reactable substrate participating interfacial polymerization for thin film composite membranes with enhanced salt rejection performance. *Desalination* **2018,** *436*, 1-7.

46. Yao, Z.; Yang, Z.; Guo, H.; Ma, X.; Dong, Y.; Tang, C. Y., Highly permeable and highly selective ultrathin film composite polyamide membranes reinforced by reactable polymer chains. *J. Colloid Interface Sci.* **2019,** *552*, 418-425.

47. She, Q.; Hou, D.; Liu, J.; Tan, K. H.; Tang, C. Y., Effect of feed spacer induced membrane deformation on the performance of pressure retarded osmosis (PRO): Implications for PRO process operation. *J. Membr. Sci.* **2013,** *445*, 170-182.

48. Lee, C.; Jang, J.; Tin, N. T.; Kim, S.; Tang, C. Y.; Kim, I. S., Effect of spacer configuration on the characteristics of FO membranes: Alteration of permeation characteristics by membrane deformation and concentration polarization. *Environ. Sci. Technol.* **2020,** *in press (https://doi.org/10.1021/acs.est.9b06921)*.

49. Li, Y.; Kłosowski, M. M.; McGilvery, C. M.; Porter, A. E.; Livingston, A. G.; Cabral, J. T., Probing flow activity in polyamide layer of reverse osmosis membrane with nanoparticle tracers. *J. Membr. Sci.* **2017,** *534*, 9-17.

50. Zhou, Z.; Hu, Y.; Boo, C.; Liu, Z.; Li, J.; Deng, L.; An, X., High-Performance Thin-Film Composite Membrane with an Ultrathin Spray-Coated Carbon Nanotube Interlayer. *Environ. Sci. Technol. Lett.* **2018,** *5*, (5), 243-248.

51. Oizerovich-Honig, R.; Raim, V.; Srebnik, S., Simulation of Thin Film Membranes Formed by Interfacial Polymerization. *Langmuir* **2010,** *26*, (1), 299-306.

52. Muscatello, J.; Müller, E. A.; Mostofi, A. A.; Sutton, A. P., Multiscale molecular simulations of the formation and structure of polyamide membranes created by interfacial polymerization. *J. Membr. Sci.* **2017,** *527*, 180-190.

53. Tang, C. Y.; Kwon, Y.-N.; Leckie, J. O., Effect of membrane chemistry and coating layer on physiochemical properties of thin film composite polyamide RO and NF membranes II. Membrane physiochemical properties and their dependence on polyamide and coating layers. *Desalination* **2009,** *242*, (1-3), 168-182.